A new technique for probing chirality via photoelectron circular dichroism

Accepted Manuscript

A new technique for probing chirality via photoelectron circular dichroism

J. Miles, D. Fernandes, A. Young, C.M.M. Bond, S.W. Crane, O. Ghafur, D. Townsend, J. Sá, J.B. Greenwood

PII: S0003-2670(17)30757-2

DOI: 10.1016/j.aca.2017.06.051

Reference: ACA 235299

To appear in: *Analytica Chimica Acta*

Received Date: 20 April 2017

Revised Date: 22 June 2017

Accepted Date: 23 June 2017

Please cite this article as: J. Miles, D. Fernandes, A. Young, C.M.M. Bond, S.W. Crane, O. Ghafur, D. Townsend, J. Sá, J.B. Greenwood, A new technique for probing chirality via photoelectron circular dichroism, *Analytica Chimica Acta* (2017), doi: 10.1016/j.aca.2017.06.051.

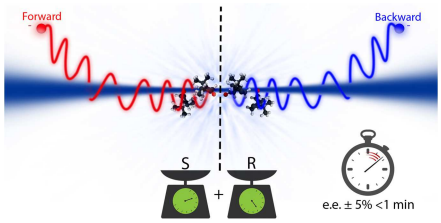

A New Technique for Probing Chirality

Supporting Information

J. Miles, D. Fernandes, A. Young, C.M.M. Bond, S. W. Crane, O. Ghafur, D. Townsend, J. Sá and J. B. Greenwood

Experimental Methods

Laser Pulses

Laser pulses at a rate of 200 kHz were produced from a Coherent titanium:sapphire Mira oscillator and RegA amplifier. Frequency doubling in a BBO crystal gave pulse energies of 125 nJ, a pulse length of 250 fs and a central wavelength of 394 nm (See Figure S1 in supplementary material). The linearly polarized pulses were converted to circular polarization using a zero-order quarter wave-plate (Halle Optics) and focused by a fused silica lens with a focal length of 15 cm. By driving a knife edge attached to a stepper motor perpendicular to the focus and measuring the transmitted intensity, a waist radius of 20 μm was measured. This corresponds to a peak intensity of 4×10^{10} Wcm^{-2} at the centre of the interaction region where it intersected the gas jet emerging from a 0.9 mm diameter capillary in one of the plates sandwiching the interaction region. The base pressure in the chamber was less than 10^{-7} mbar rising to a few 10^{-6} mbar during measurements.

To measure the degree of circular polarization, the method of Schaefer et al.[1] was used to determine the Stokes S_3 parameter. For this method a second quarter waveplate was placed after the first one and the power transmission through a Glan-laser polarizing prism measured as a function of the angle of the second waveplate using a photodiode. This can be expressed in terms of the Stokes parameters which fully describe the polarization state of the pulses.

$$I(\theta) = \frac{1}{2}(A + B\sin 2\theta + C\cos 4\theta + D\sin 4\theta) \qquad (3)$$

$$A = S_0 + \frac{S_1}{2},\ B = S_3,\ \ C = \frac{S_1}{2},\ D = \frac{S_2}{2}$$

A typical measurement, shown in Figure S2, has been fitted with the above expression from which a value of $S_3 = 0.993$ was obtained showing that our pulses possessed a high degree of circular polarization.

Magnetic Field

The magnetic field was generated in the instrument using a pair of coils with 320 turns, a radius of 69 mm and separation distance of 135mm. For the present results, a current of 1.5-2.0 A was passed through the coils generating a B-field of 30-40 Gauss in the interaction region. At a B-field strength of 30 Gauss, the Larmor radius of an electron with kinetic energy of 0.77 eV (the excess energy from 2 + 1 REMPI of camphor at 394 nm using an ionisation energy of 8.7eV [2]) is 1.0 mm. The repeller and extraction plates sandwiching the interaction region are separated by 10 mm while the apertures seen by the electrons as they emerge from the interaction region have a diameter of 9 mm. Therefore, the electrons' maximum Larmor diameter is well within these dimensions ensuring none of the electrons impinge on these plates. Similarly the **E** × **B** deflection plates have a separation of 15 mm to avoid collisions. The front sections of the two channel electron multipliers (Photonis CEM 5901 Magnum) used for the electron detection were biased with a +500 V potential to accelerate the electrons onto an active area of 9 mm diameter. The voltages of the deflection plates were varied so that all the electrons were hitting the active area of the detector. To validate this supposition, the magnetic field was increased from 30 to 40 Gauss with concomitant adjustment of the deflection plate potentials. This reduction in the electrons' Larmor radius produced no change in the G-value for both fenchone and camphor within the statistical uncertainties.

With a magnetic field of 30 Gauss, simulations show that transmission of all the photoelectrons is achievable for emission energies up to 3.5 eV. This upper limit can be extended to higher energies if a larger magnetic field is used to reduce the Larmor radius. This would allow collection of all photoelectrons even if a short wavelength light source such as from a synchrotron were used. However, since the PECD asymmetry changes (and can reverse) for ionisation of different electronic and vibrational states and it is the low energy electrons which are most sensitive to the chiral potential, it desirable to choose a wavelength which just exceeds the ionisation threshold. In this way the maximum asymmetry can usually be achieved.

The application of the magnetic field ensures that there is 100% confinement of the emitted electrons. Due to a slight dip in the magnetic field strength at the interaction region, electrons with emission angles in the range 89.5-90.5° can be trapped in a weak magnetic mirror. However, these electrons constitute less than 1% of the solid angle and have a negligible contribution to the asymmetry since the odd terms in equation (1) depend on $\cos\theta$. Similarly, very low energy electrons (< 5 meV) which are susceptible to stray electric fields and non-uniformities in the magnetic field may fail to reach a detector.

Samples

All samples were purchased from Sigma-Aldrich and used without further purification. The quoted purities for these samples were R-Camphor 98%, S-Camphor 99%, R-Fenchone 98% (this purity is questionable, see main paper), and S-Fenchone 99.5%. To create samples with a range of enantiomer excesses, equal quantities (200μg) of the R- and S-enantiomers were measured with an accurate microbalance (Metler Toledo AT20), dissolved in 2 ml of acetone, and mixed in set ratios with a pipette of μL precision. Evaporation of the solvent left a sample with well-mixed samples of defined enantiomer excess.

Data Acquisition

The two channel electron multipliers were operated in counting mode and the raw count rate in each was monitored to ensure an average of less than 0.1 electrons were detected in each per laser pulse. G-values with σ of around 0.2% were obtained from 20 seconds of acquisition for each polarization state and repeated 20 times. Differences in the efficiencies of the two electron detectors had the potential to introduce instrumental asymmetry to the measurements. Therefore G has been defined so that the detector efficiencies cancel out in equation 2. The main source of uncertainty in the measurements originates from variations in the laser power and target gas pressure between changes in the polarization state.

Mass spectra were obtained before and after the stereo-electron detection measurements by biassing one of the plates in the interaction region (repeller) to +4 kV and the other (extraction) to +2.9 kV. Mass spectra for camphor and fenchone are shown in Figure S3. Since a low laser intensity was used, the spectrum is dominated by the parent ion ($C_{10}H_{16}O^+$, 152 amu) with a small contribution from fragment ions identified as $C_6H_9{}^+$ in both molecules, and $C_7H_{11}{}^+$ in camphor. There are no other masses in the spectrum confirming that our measurements of G contain no photoelectrons originating from background gas or other contaminants.

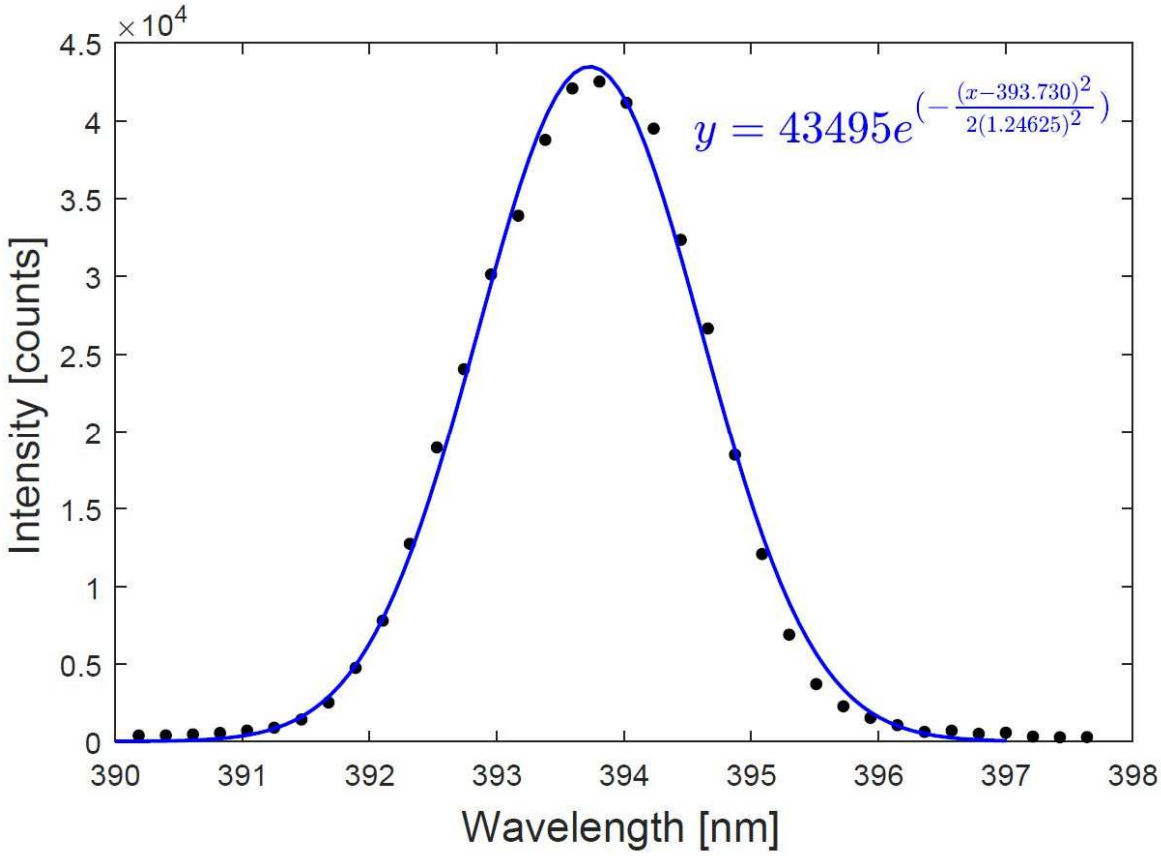

Figure S1: Spectrum of the 2nd harmonic laser pulses measured with an Ocean Optics USB4000 spectrometer, fitted with a gaussian profile. The bandwidth is 2.1 nm at full width half maximum.

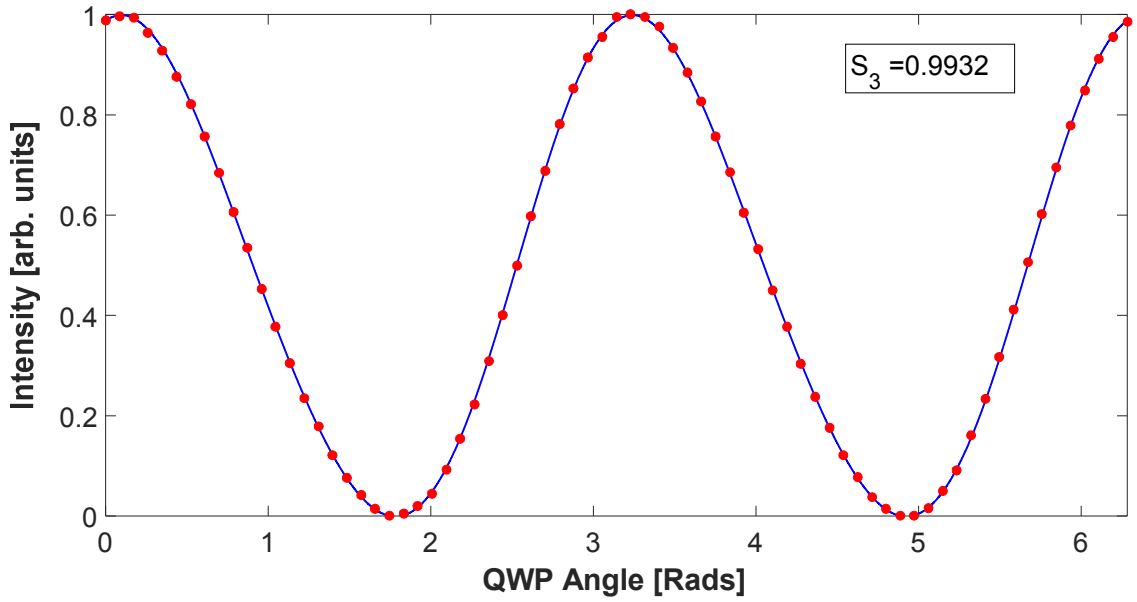

Figure S2: Transmitted laser power as a function of analysing waveplate angle fitted using Equation 3 to determine the Stokes parameters.

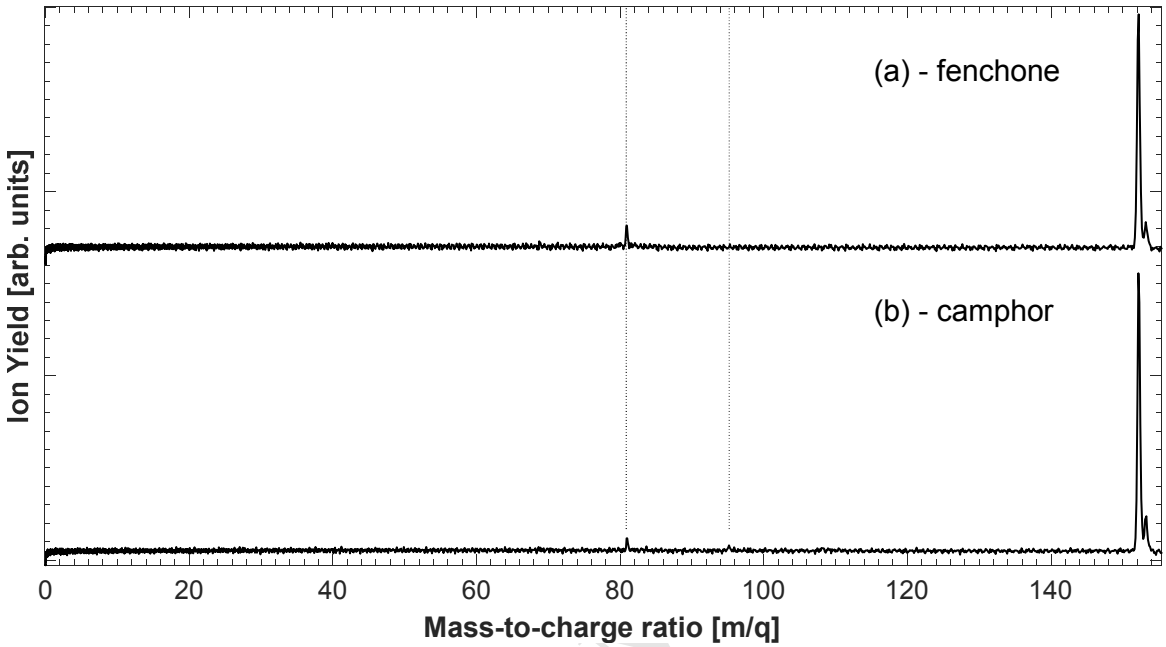

Figure S3: Mass spectra obtained for (a) fenchone and (b) camphor which have been shifted relative to each other for clarity. These are dominated by the parent ion $C_{10}H_{16}O^{+}$ at 152u (with an isotope peak at 153u) while fragment ions at 81u and 95u can be attributed to $C_6H_9{}^{+}$ in both molecules, and $C_7H_{11}{}^{+}$ in camphor, respectively.

Appendix A

Numerical data for Figure 2 (main paper)

Enantiomer Excess (%)	G (%)	ΔG (2σ)
-100	-8.6814	0.41601
-60	-5.4657	0.53682
-33	-3.4493	0.44962
-30	-3.0737	0.6458
-2.5	-0.5584	0.74914
0	0.18023	0.79603
30	2.1077	0.73278
33	2.7446	0.53429

60.8	5.1239	0.23338
100	8.0946	0.51336

Numerical data for Figure S2

QWP Angle [Rads]	Intensity [Arb. Units]
0	0.14929
0.087266	0.15064
0.17453	0.15012
0.2618	0.14538
0.34907	0.13984
0.43633	0.13172
0.5236	0.12289
0.61087	0.11283
0.69813	0.1014
0.7854	0.089133
0.87266	0.077823
0.95993	0.064802
1.0472	0.052963
1.1345	0.041457
1.2217	0.030487
1.309	0.021564
1.3963	0.012552
1.4835	0.005342
1.5708	1.81E-05
1.6581	-0.00434
1.7453	-0.00651
1.8326	-0.00599
1.9199	-0.00353
2.0071	0.00045
2.0944	0.008058
2.1817	0.017719
2.2689	0.028395
2.3562	0.042162
2.4435	0.056577
2.5307	0.072204
2.618	0.0878
2.7053	0.10208
2.7925	0.11673
2.8798	0.1279
2.9671	0.13779
3.0543	0.14423
3.1416	0.1504
3.2289	0.15119
3.3161	0.15041
3.4034	0.14731
3.4907	0.1408
3.5779	0.13293
3.6652	0.12381
3.7525	0.11288
3.8397	0.10148
3.927	0.088875
4.0143	0.077371
4.1015	0.064281
4.1888	0.052857
4.2761	0.04123
4.3633	0.030882
4.4506	0.021235
4.5379	0.012457
4.6251	0.005621
4.7124	-0.00073
4.7997	-0.00441
4.8869	-0.00662
4.9742	-0.00664
5.0615	-0.00404
5.1487	0.001284
5.236	0.007815
5.3233	0.018758
5.4105	0.030167
5.4978	0.04349
5.5851	0.058298
5.6723	0.073276
5.7596	0.088338
5.8469	0.10308
5.9341	0.11628
6.0214	0.1274
6.1087	0.13716
6.1959	0.14427
6.2832	0.14882

Numerical data for Figure S3

Mass/charge (u)	Ion Yield Camphor	Mass/charge (u)	Ion Yield Fenchone
79.94	2.46	79.98	3.58
80.03	2.93	80.08	2.94
80.13	2.09	80.18	3.06
80.23	2.91	80.28	3.15
80.33	2.16	80.39	3.04
80.42	3.00	80.49	2.89
80.52	3.12	80.59	2.67
80.62	2.35	80.69	3.15
80.72	2.62	80.79	5.73
80.81	3.31	80.90	8.27
80.91	5.88	81.00	7.39
81.01	5.86	81.10	3.78
81.11	4.60	81.20	2.84
81.20	3.39	81.31	2.76
81.30	2.63	81.41	2.07
81.40	2.44	81.51	3.70
81.50	2.95	81.62	3.06
81.59	2.57	81.72	3.22
81.69	3.07	81.82	3.08
81.79	2.92	81.92	2.81
81.89	2.40	82.03	2.96
81.99	3.12	82.13	2.83
82.09	2.22	82.23	2.83
82.18	2.94	82.34	3.67
82.28	2.59	82.44	3.07
82.38	3.14	82.54	2.68
82.48	2.90	82.65	2.38
82.58	2.05	82.75	2.71
82.68	2.19	82.86	3.67
82.78	2.66	82.96	2.72
82.87	2.88	83.06	2.88
82.97	3.18	83.17	3.17
83.07	2.78	83.27	2.62
83.17	2.93	83.37	2.72
83.27	2.81	83.48	2.05
83.37	1.97	83.58	3.52
83.47	2.81	83.69	3.38
83.57	2.63	83.79	3.01
83.67	3.68	83.90	2.42
83.77	2.79	84.00	2.81
83.86	2.32	84.10	2.74
83.96	2.77	84.21	3.14
84.06	2.57	84.31	2.60
84.16	2.66	84.42	3.46
84.26	2.35	84.52	3.32
84.36	2.83	84.63	2.83
84.46	3.01	84.73	2.56
84.56	2.26	84.84	2.50
84.66	1.80	84.94	3.59
84.76	2.66	85.05	2.94
84.86	2.62	85.15	3.04
84.96	3.17	85.26	3.16
85.06	2.45	85.36	2.57
85.16	2.37	85.47	2.75
85.26	2.88	85.57	2.29
85.36	2.05	85.68	3.21
85.46	2.80	85.78	3.29
85.56	2.62	85.89	2.73
85.66	3.07	86.00	2.36
85.76	3.17	86.10	2.59
85.86	2.13	86.21	2.20
85.96	2.52	86.31	2.96
86.06	2.47	86.42	2.16
86.17	2.42	86.52	3.54
86.27	2.86	86.63	2.93
86.37	2.82	86.74	2.39
86.47	2.71	86.84	2.39
86.57	2.37	86.95	2.36
86.67	1.86	87.06	3.52
86.77	2.83	87.16	2.97
86.87	2.23	87.27	2.62
86.97	2.84	87.37	3.05
87.07	2.54	87.48	2.61
87.18	2.13	87.59	2.49
87.28	2.76	87.69	2.27
87.38	1.81	87.80	2.88
87.48	2.61	87.91	3.41
87.58	2.75	88.01	2.73
87.68	3.13	88.12	2.03
87.78	2.84	88.23	2.60
87.89	2.05	88.34	2.40
87.99	2.44	88.44	3.16
88.09	2.80	88.55	2.16
88.19	2.42	88.66	3.02
88.29	2.70	88.76	3.01
88.40	2.77	88.87	2.25
88.50	2.63	88.98	2.30
88.60	2.57	89.09	2.27
88.70	1.57	89.19	3.36
88.80	2.91	89.30	3.12
88.91	2.50	89.41	2.58
89.01	3.21	89.52	2.75
89.11	2.44	89.63	2.64
89.21	2.13	89.73	2.43
89.32	2.53	89.84	2.76
89.42	2.23	89.95	2.72
89.52	2.27	90.06	3.40
89.62	2.67	90.17	2.99
89.73	2.85	90.27	2.11
89.83	2.82	90.38	2.77
89.93	2.22	90.49	2.20
90.03	2.04	90.60	3.26
90.14	2.72	90.71	2.47
90.24	2.49	90.82	3.06
90.34	3.10	90.92	2.94
90.45	2.66	91.03	2.21
90.55	2.48	91.14	2.27
90.65	2.73	91.25	2.64
90.76	1.95	91.36	2.95
90.86	2.98	91.47	3.09
90.96	2.65	91.58	2.56
91.07	2.78	91.69	2.71
91.17	2.73	91.80	2.80
91.27	2.21	91.90	2.24
91.38	2.23	92.01	2.85
91.48	2.16	92.12	2.82
91.59	2.30	92.23	3.56
91.69	3.03	92.34	2.73
91.79	2.75	92.45	2.05
91.90	2.41	92.56	2.80
92.00	2.14	92.67	2.46
92.11	1.95	92.78	3.18
92.21	2.95	92.89	2.56
92.31	2.08	93.00	2.90
92.42	2.80	93.11	3.03
92.52	2.81	93.22	2.51
92.63	2.29	93.33	1.97
92.73	2.69	93.44	2.97
92.84	1.75	93.55	2.93
92.94	2.98	93.66	3.41
93.05	2.83	93.77	2.42
93.15	2.91	93.88	2.53
93.25	2.54	93.99	2.76
93.36	2.27	94.10	2.30
93.46	2.32	94.21	2.88
93.57	2.90	94.32	2.71
93.67	2.17	94.43	3.06
93.78	2.95	94.54	2.96
93.88	2.78	94.66	2.02
93.99	2.39	94.77	2.64
94.09	2.28	94.88	2.68
94.20	1.76	94.99	3.25
94.31	2.83	95.10	3.05
94.41	2.51	95.21	2.86
94.52	3.03	95.32	2.82
94.62	2.75	95.43	2.65
94.73	2.30	95.54	2.12
94.83	2.63	95.66	3.11
94.94	2.98	95.77	2.71
95.04	3.32	95.88	3.12
95.15	4.00	95.99	2.61
95.26	3.45	96.10	2.48
95.36	3.15	96.21	2.85
95.47	2.68	96.33	1.96
95.57	2.29	96.44	2.89
95.68	2.85	96.55	2.96
95.79	2.33	96.66	3.03
95.89	3.49	96.77	2.85
96.00	2.77	96.89	2.13
96.10	2.22	97.00	2.68
96.21	2.50	97.11	2.87
96.32	2.19	97.22	2.72
96.42	2.98	97.33	2.83
96.53	2.40	97.45	2.74
96.64	2.59	97.56	2.67
96.74	2.86	97.67	2.62
96.85	2.37	97.78	1.77
96.96	2.27	97.90	3.34
97.06	2.56	98.01	2.73
97.17	2.52	98.12	3.33
97.28	3.24	98.24	2.50
97.39	2.54	98.35	2.41

97.49	2.39	98.46	2.66
97.60	2.62	98.58	2.38
97.71	2.11	98.69	2.69
97.81	3.19	98.80	3.04
97.92	2.16	98.91	2.91
98.03	3.01	99.03	2.63
98.14	3.20	99.14	2.03
98.24	2.15	99.26	2.44
98.35	2.39	99.37	2.86
98.46	1.95	99.48	2.63
98.57	2.87	99.60	3.13
98.67	2.73	99.71	2.92
98.78	2.62	99.82	2.63
98.89	2.67	99.94	2.68
99.00	2.27	100.05	2.00
99.11	2.17	100.16	3.33
99.21	2.53	100.28	2.87
99.32	2.35	100.39	3.00
99.43	2.93	100.51	2.61
99.54	2.84	100.62	2.58
99.65	2.30	100.74	2.70
99.76	2.73	100.85	2.39
99.86	1.94	100.96	2.72
99.97	2.83	101.08	3.48
100.08	2.37	101.19	2.83
100.19	3.24	101.31	2.39
100.30	2.75	101.42	2.22
100.41	2.22	101.54	2.65
100.51	2.24	101.65	3.39
100.62	2.68	101.77	2.54
100.73	2.62	101.88	2.80
100.84	2.79	102.00	2.99
100.95	2.59	102.11	2.45
101.06	2.70	102.23	2.60
101.17	2.48	102.34	1.73
101.28	1.79	102.46	3.22
101.39	2.54	102.57	3.18
101.50	2.33	102.69	3.01
101.61	3.14	102.80	2.44
101.71	2.59	102.92	2.54
101.82	1.89	103.04	2.76
101.93	2.51	103.15	3.06
102.04	2.09	103.27	2.36
102.15	2.61	103.38	3.35
102.26	2.49	103.50	2.89
102.37	2.66	103.61	2.43
102.48	3.11	103.73	2.40
102.59	2.34	103.85	2.12
102.70	2.04	103.96	3.52
102.81	2.64	104.08	2.62
102.92	2.64	104.20	2.91
103.03	3.21	104.31	2.70
103.14	2.42	104.43	2.53
103.25	2.39	104.54	2.52
103.36	2.69	104.66	2.17
103.47	1.86	104.78	3.16
103.58	2.60	104.89	3.14
103.69	2.30	105.01	2.79
103.80	2.86	105.13	2.41
103.91	2.73	105.24	2.62
104.03	1.84	105.36	2.20
104.14	2.42	105.48	3.06
104.25	2.23	105.60	2.30
104.36	2.61	105.71	3.53
104.47	2.80	105.83	2.96
104.58	2.75	105.95	2.41
104.69	2.65	106.06	2.32
104.80	2.32	106.18	2.51
104.91	2.04	106.30	3.26
105.02	2.82	106.42	2.83
105.14	2.41	106.53	2.44
105.25	2.95	106.65	2.95
105.36	2.85	106.77	2.51
105.47	2.41	106.89	2.49
105.58	2.71	107.01	2.32
105.69	2.03	107.12	2.89
105.80	2.57	107.24	3.54
105.92	2.60	107.36	2.64
106.03	2.98	107.48	2.19
106.14	2.59	107.60	2.52
106.25	1.94	107.71	2.57
106.36	2.24	107.83	3.38
106.47	2.47	107.95	2.34
106.59	2.34	108.07	3.31
106.70	2.46	108.19	3.18
106.81	2.67	108.31	2.32
106.92	2.55	108.42	2.21
107.03	2.49	108.54	2.20
107.15	1.59	108.66	3.31
107.26	2.77	108.78	3.07
107.37	2.44	108.90	2.73
107.48	3.22	109.02	2.86
107.60	2.63	109.14	2.63
107.71	2.16	109.26	2.62
107.82	2.94	109.38	2.63
107.93	2.51	109.49	2.75
108.05	3.27	109.61	3.19
108.16	3.23	109.73	2.76
108.27	3.24	109.85	2.17
108.39	3.09	109.97	2.95
108.50	2.36	110.09	2.28
108.61	2.00	110.21	3.41
108.73	2.64	110.33	2.47
108.84	2.59	110.45	3.32
108.95	3.19	110.57	2.91
109.06	2.94	110.69	2.30
109.18	2.67	110.81	2.30
109.29	2.92	110.93	2.69
109.40	1.77	111.05	3.02
109.52	2.93	111.17	3.00
109.63	2.46	111.29	2.49
109.75	2.75	111.41	2.62
109.86	2.81	111.53	2.61
109.97	2.20	111.65	2.17
110.09	2.71	111.77	2.66
110.20	2.33	111.89	2.67
110.31	2.53	112.01	3.46
110.43	3.19	112.13	2.69
110.54	3.02	112.25	2.10
110.66	2.63	112.37	2.72
110.77	2.22	112.50	2.55
110.89	2.26	112.62	3.11
111.00	2.86	112.74	2.56
111.11	2.33	112.86	3.04
111.23	2.68	112.98	2.95
111.34	2.90	113.10	2.40
111.46	2.30	113.22	2.03
111.57	2.53	113.34	2.74
111.69	1.74	113.46	3.01
111.80	2.59	113.59	3.44
111.92	2.60	113.71	2.35
112.03	2.81	113.83	2.43
112.15	2.48	113.95	2.70
112.26	2.19	114.07	2.16
112.38	2.41	114.19	2.88
112.49	2.60	114.32	2.62
112.61	2.24	114.44	3.12
112.72	2.97	114.56	2.81
112.84	2.84	114.68	1.92
112.95	2.40	114.80	2.58
113.07	2.46	114.93	2.36
113.18	1.93	115.05	3.02
113.30	2.96	115.17	2.93
113.41	2.51	115.29	2.99
113.53	3.04	115.41	2.85
113.64	2.70	115.54	2.35
113.76	2.07	115.66	2.23
113.88	2.45	115.78	3.19
113.99	2.03	115.90	2.77
114.11	2.41	116.03	3.19
114.22	2.59	116.15	2.61
114.34	2.57	116.27	2.58
114.46	2.66	116.40	2.74
114.57	2.38	116.52	2.15
114.69	2.04	116.64	2.83
114.80	2.58	116.76	2.77
114.92	2.11	116.89	2.89
115.04	3.19	117.01	2.52
115.15	2.58	117.13	1.83
115.27	2.23	117.26	2.57
115.39	2.41	117.38	2.76
115.50	2.16	117.50	2.84
115.62	2.87	117.63	2.74
115.74	2.42	117.75	2.83
115.85	2.68	117.88	2.69
115.97	2.93	118.00	2.61
116.09	2.22	118.12	1.78
116.20	2.12	118.25	3.28
116.32	2.10	118.37	2.79
116.44	2.64	118.49	3.40
116.55	3.03	118.62	2.44
116.67	2.50	118.74	2.33
116.79	2.24	118.87	2.84
116.91	2.44	118.99	2.40
117.02	2.03	119.12	2.85
117.14	2.66	119.24	3.00
117.26	2.00	119.36	2.91
117.38	2.78	119.49	2.76

117.49	2.89	119.61	2.12	128.19	2.04	130.96	2.80
117.61	2.16	119.74	2.31	128.32	2.44	131.09	3.37
117.73	2.20	119.86	2.96	128.44	2.52	131.22	2.80
117.85	1.97	119.99	2.63	128.56	2.83	131.35	2.13
117.96	2.71	120.11	3.01	128.68	2.74	131.48	2.70
118.08	2.71	120.24	2.73	128.81	2.11	131.61	2.06
118.20	2.96	120.36	2.38	128.93	2.04	131.74	3.23
118.32	2.89	120.49	2.64	129.05	2.54	131.87	2.30
118.44	2.41	120.61	1.99	129.18	2.39	132.01	3.21
118.55	2.21	120.74	3.31	129.30	2.82	132.14	2.86
118.67	2.57	120.86	2.75	129.42	2.77	132.27	2.22
118.79	2.39	120.99	2.94	129.55	2.25	132.40	2.29
118.91	2.95	121.11	2.72	129.67	2.53	132.53	2.50
119.03	2.57	121.24	2.42	129.79	1.77	132.66	3.13
119.15	2.05	121.36	2.69	129.92	2.83	132.79	3.04
119.26	2.56	121.49	2.48	130.04	2.36	132.92	2.37
119.38	1.82	121.62	2.69	130.17	2.82	133.05	2.65
119.50	2.73	121.74	3.41	130.29	2.76	133.19	2.69
119.62	2.15	121.87	2.87	130.41	2.01	133.32	2.18
119.74	3.15	121.99	2.68	130.54	2.35	133.45	2.66
119.86	2.70	122.12	2.17	130.66	2.15	133.58	2.67
119.98	1.89	122.24	2.48	130.79	2.39	133.71	3.59
120.09	2.26	122.37	3.03	130.91	2.99	133.84	2.67
120.21	2.33	122.50	2.45	131.03	2.76	133.98	2.01
120.33	2.65	122.62	2.80	131.16	2.56	134.11	2.77
120.45	2.63	122.75	2.91	131.28	2.11	134.24	2.44
120.57	2.47	122.87	2.49	131.41	1.92	134.37	3.31
120.69	2.66	123.00	2.78	131.53	2.93	134.50	2.59
120.81	2.42	123.13	1.90	131.66	2.16	134.64	2.83
120.93	1.87	123.25	3.28	131.78	2.77	134.77	2.91
121.05	2.60	123.38	2.84	131.90	2.79	134.90	2.23
121.17	2.43	123.51	2.92	132.03	2.21	135.03	1.99
121.29	3.39	123.63	2.41	132.15	2.50	135.17	2.76
121.41	2.52	123.76	2.46	132.28	1.65	135.30	2.93
121.53	2.05	123.89	2.72	132.40	2.65	135.43	3.42
121.65	2.68	124.01	2.84	132.53	2.63	135.56	2.45
121.76	2.21	124.14	2.39	132.65	2.90	135.70	2.61
121.88	2.69	124.27	3.23	132.78	2.53	135.83	2.77
122.00	2.26	124.40	2.85	132.90	2.12	135.96	2.39
122.12	2.81	124.52	2.42	133.03	2.21	136.09	3.09
122.24	2.92	124.65	2.28	133.15	2.69	136.23	2.80
122.36	2.08	124.78	2.19	133.28	2.11	136.36	3.25
122.48	1.79	124.90	3.32	133.40	2.69	136.49	2.84
122.60	2.28	125.03	2.68	133.53	2.68	136.63	1.94
122.72	2.44	125.16	2.94	133.65	2.44	136.76	2.68
122.84	2.99	125.29	2.86	133.78	2.44	136.89	2.27
122.96	2.42	125.41	2.57	133.91	1.74	137.03	3.19
123.09	2.48	125.54	2.54	134.03	2.89	137.16	2.79
123.21	2.61	125.67	1.96	134.16	2.42	137.29	2.96
123.33	1.85	125.80	3.17	134.28	2.97	137.43	2.58
123.45	2.50	125.92	3.13	134.41	2.53	137.56	2.35
123.57	2.26	126.05	2.76	134.53	2.17	137.69	2.09
123.69	2.93	126.18	2.45	134.66	2.44	137.83	3.04
123.81	2.90	126.31	2.65	134.79	2.09	137.96	2.76
123.93	1.93	126.44	2.29	134.91	2.59	138.10	3.14
124.05	2.58	126.56	2.79	135.04	2.59	138.23	2.41
124.17	2.22	126.69	2.15	135.16	2.56	138.36	2.41
124.29	2.67	126.82	3.54	135.29	2.51	138.50	2.79
124.41	2.72	126.95	2.70	135.42	2.36	138.63	2.17
124.53	2.70	127.08	2.34	135.54	1.88	138.77	2.97
124.66	2.67	127.21	2.40	135.67	2.56	138.90	2.78
124.78	2.17	127.33	2.38	135.80	2.01	139.03	3.40
124.90	1.84	127.46	3.51	135.92	3.15	139.17	2.76
125.02	2.73	127.59	2.66	136.05	2.54	139.30	2.15
125.14	2.26	127.72	2.65	136.18	2.17	139.44	2.72
125.26	2.85	127.85	3.05	136.30	2.37	139.57	2.67
125.38	2.54	127.98	2.33	136.43	1.98	139.71	2.73
125.50	2.20	128.11	2.39	136.56	2.81	139.84	2.96
125.63	2.61	128.24	2.00	136.68	2.34	139.98	2.77
125.75	1.76	128.37	3.00	136.81	2.67	140.11	2.69
125.87	2.59	128.49	3.48	136.94	2.99	140.25	2.46
125.99	2.44	128.62	2.77	137.06	2.22	140.38	1.73
126.11	3.04	128.75	2.11	137.19	2.39	140.52	3.19
126.23	2.70	128.88	2.43	137.32	2.18	140.65	2.55
126.36	2.01	129.01	2.42	137.44	2.57	140.79	3.31
126.48	2.40	129.14	2.98	137.57	3.13	140.92	2.37
126.60	2.56	129.27	2.21	137.70	2.60	141.06	2.30
126.72	2.33	129.40	3.12	137.83	2.30	141.19	2.71
126.85	2.60	129.53	2.91	137.95	2.41	141.33	2.41
126.97	2.62	129.66	2.35	138.08	2.04	141.46	2.81
127.09	2.70	129.79	2.21	138.21	2.62	141.60	2.96
127.21	2.52	129.92	2.35	138.34	2.01	141.73	2.91
127.33	1.47	130.05	3.26	138.46	2.72	141.87	2.89
127.46	2.76	130.18	3.01	138.59	2.88	142.01	2.09
127.58	2.31	130.31	2.63	138.72	2.06	142.14	2.38
127.70	3.11	130.44	2.71	138.85	2.35	142.28	2.81
127.82	2.29	130.57	2.61	138.97	1.91	142.41	2.76
127.95	2.08	130.70	2.55	139.10	2.80	142.55	3.05
128.07	2.57	130.83	2.44	139.23	2.55	142.69	2.76

139.36	2.62	142.82	2.45
139.49	2.83	142.96	2.56
139.62	2.17	143.09	2.06
139.74	2.14	143.23	3.25
139.87	2.51	143.37	2.76
140.00	2.41	143.50	3.02
140.13	2.91	143.64	2.43
140.26	2.66	143.78	2.27
140.39	2.23	143.91	2.53
140.51	2.57	144.05	2.16
140.64	1.86	144.19	2.69
140.77	2.70	144.32	3.28
140.90	2.13	144.46	2.97
141.03	3.08	144.60	2.60
141.16	2.74	144.73	2.11
141.29	1.94	144.87	2.39
141.42	2.21	145.01	3.16
141.54	2.24	145.15	2.56
141.67	2.57	145.28	2.90
141.80	2.39	145.42	3.00
141.93	2.46	145.56	2.43
142.06	2.63	145.69	2.64
142.19	2.40	145.83	1.75
142.32	1.90	145.97	3.34
142.45	2.50	146.11	2.83
142.58	2.40	146.25	2.97
142.71	3.25	146.38	2.44
142.84	2.56	146.52	2.27
142.97	2.03	146.66	2.66
143.10	2.66	146.80	2.70
143.23	2.20	146.94	2.47
143.36	2.77	147.07	3.22
143.49	2.23	147.21	2.69
143.62	2.81	147.35	2.41
143.75	2.91	147.49	2.28
143.88	2.15	147.63	2.08
144.01	1.99	147.76	3.36
144.14	2.35	147.90	2.67
144.27	2.44	148.04	2.92
144.40	3.00	148.18	2.85
144.53	2.28	148.32	2.39
144.66	2.41	148.46	2.66
144.79	2.56	148.60	2.17
144.92	1.79	148.74	3.16
145.05	2.66	148.88	3.14
145.18	2.08	149.01	2.76
145.31	2.88	149.15	2.43
145.44	2.90	149.29	2.48
145.57	2.00	149.43	2.42
145.71	2.57	149.57	2.73
145.84	2.17	149.71	2.32
145.97	2.61	149.85	3.32
146.10	2.53	149.99	2.79
146.23	2.76	150.13	2.34
146.36	2.79	150.27	2.26
146.49	2.30	150.41	2.22
146.62	1.95	150.55	3.26
146.75	2.83	150.69	2.59
146.89	2.54	150.83	2.55
147.02	2.69	150.97	3.20
147.15	2.49	151.11	2.67
147.28	2.25	151.25	2.87
147.41	2.57	151.39	2.21
147.54	1.85	151.53	3.35
147.68	2.50	151.67	4.68
147.81	2.57	151.81	7.21
147.94	3.08	151.95	19.38
148.07	2.59	152.09	58.80
148.20	1.85	152.23	80.76
148.34	2.31	152.37	46.53
148.47	2.43	152.51	18.59
148.60	2.52	152.65	6.78
148.73	2.45	152.79	4.28
148.87	2.80	152.93	4.42
149.00	2.66	153.07	8.75
149.13	2.35	153.22	12.62
149.26	1.67	153.36	10.13
149.40	2.81	153.50	5.64
149.53	2.39	153.64	3.70
149.66	3.17	153.78	3.31
149.79	2.51	153.92	2.80
149.93	2.19	154.06	2.39
150.06	2.72	154.20	2.47
150.19	2.05	154.35	2.45
150.33	2.62	154.49	2.82
150.46	2.56	154.63	2.44
150.59	2.70	154.77	1.91
150.72	2.89	154.91	2.38
150.86	2.06	155.05	2.03
150.99	2.05	155.20	3.08
151.12	2.64	155.34	1.85
151.26	2.46	155.48	3.04
151.39	3.02	155.62	2.70
151.52	2.53	155.76	2.50
151.66	2.94	155.91	2.62
151.79	5.96	156.05	3.05
151.93	16.18	156.19	3.58
152.06	43.39	156.33	3.26
152.19	77.82	156.48	2.93
152.33	69.92	156.62	3.16
152.46	37.11	156.76	3.02
152.59	16.57	156.90	2.52
152.73	9.36	157.05	2.84
152.86	5.69	157.19	3.03
153.00	6.68	157.33	3.72
153.13	11.01	157.48	2.64
153.27	11.87	157.62	1.73
153.40	8.57	157.76	2.38
153.53	5.41	157.90	1.92
153.67	3.81	158.05	2.64
153.80	3.73	158.19	2.00
153.94	2.51	158.33	2.53
154.07	2.89	158.48	2.68
154.21	2.81	158.62	2.30
154.34	1.89	158.77	1.87
154.48	2.09	158.91	2.20
154.61	1.37	159.05	2.50
154.75	2.53	159.20	2.20
154.88	2.51	159.34	1.01
155.02	2.87	159.48	0.63
155.15	2.33	159.63	0.63
155.29	1.92	159.77	0.37
155.42	1.99	159.92	0.50
155.56	2.42	160.06	0.58
155.69	2.43	160.20	0.62
155.83	3.35	160.35	0.42
155.96	3.49	160.49	0.36
156.10	3.33	160.64	0.39
156.24	2.97	160.78	0.35
156.37	2.22		
156.51	2.97		
156.64	2.35		
156.78	3.06		
156.91	2.70		
157.05	2.30		
157.19	2.68		
157.32	2.07		
157.46	2.34		
157.59	2.20		
157.73	1.94		
157.87	2.04		
158.00	1.75		
158.14	1.62		
158.28	2.34		
158.41	2.31		
158.55	3.42		
158.69	2.66		
158.82	1.97		
158.96	1.32		
159.10	0.51		
159.23	0.55		
159.37	0.38		
159.51	0.36		
159.64	0.41		
159.78	0.34		
159.92	0.25		
160.06	0.12		

Supplementary References

[1] B. Schaefer, E. Collett, R. Smyth, D. Barrett and B. Fraher, Measuring the Stokes polarization parameters, *Am. J. Phys.*, **75**, 163 (2007)
[2] E. E. Rennie, I.Powis, U. Hergenhahn, O. Kugeler, G. Garcia, T. Lischke, S. Marburger, Valence and C 1s core level photoelectron spectra of camphor, *J. Electron Spectrosc. Relat. Phenom*., **125**, 197–203 (2002)

ToF MCP Detector

B Field (<40 Gauss)

Ion extraction plates

Trochoidal Deflection Plates

Forward Electron Detector

Backward Electron Detector

394nm Laser

Gas Jet

150mm

Interaction region

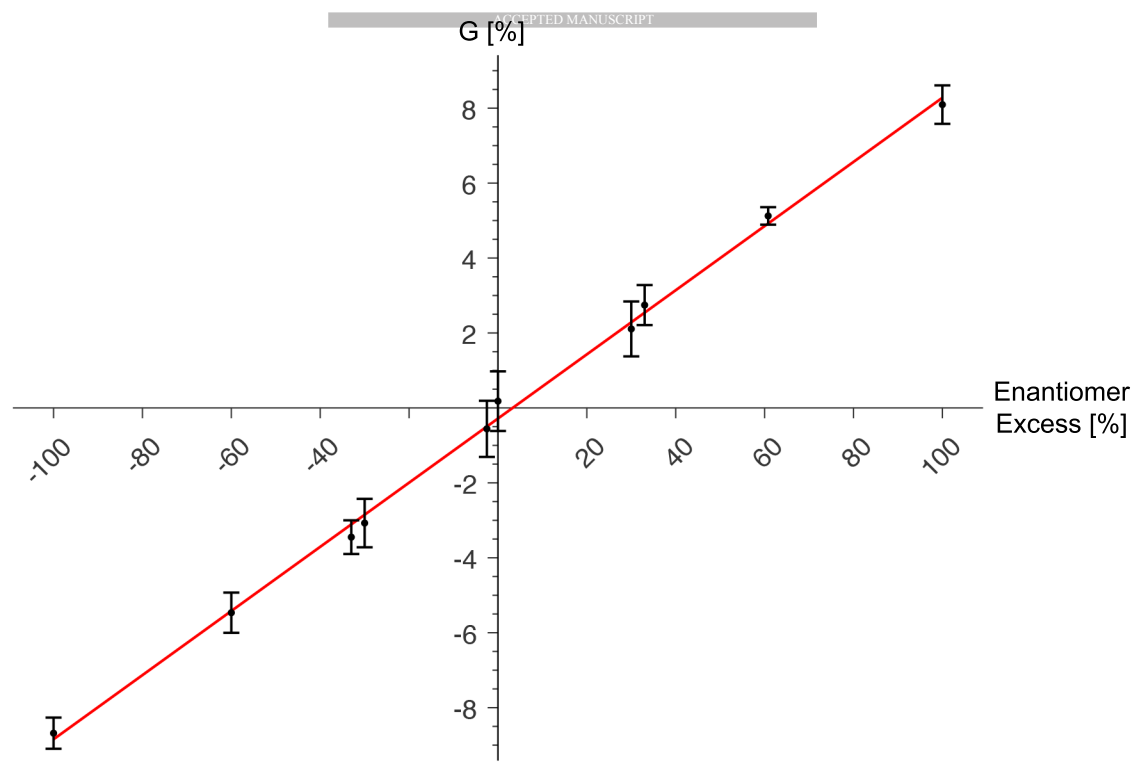

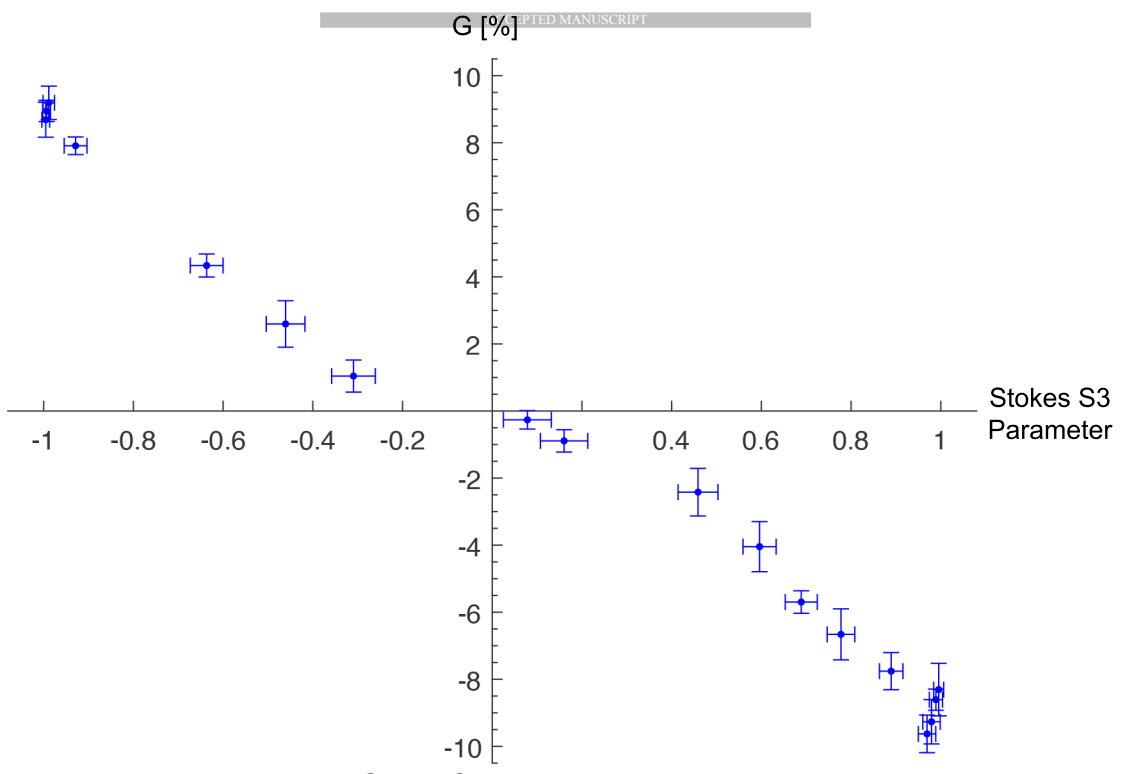

- Chiral analysis remains a challenging proposition in modern analytical chemistry
- The phenomenon of Photoelectron Circular Dichroism offers a route to faster more sensitive analysis
- Electrons are ionised with circular polarized femtosecond laser pulses
- The asymmetry in electron angular emission is measured with a novel stereo-detection system
- In identifying chiral molecules, speed and sensitivity equivalent to mass spectrometry can be achieved

A New Technique for Probing Chirality via Photoelectron Circular Dichroism

J. Miles[a], D. Fernandes[b], A. Young[a], C. M. M. Bond[a], S. W. Crane[d], O. Ghafur[d], D. Townsend[d,e] , J. Sá[b,c] and J. B. Greenwood[a,†]

a. Centre for Plasma Physics, School of Mathematics and Physics, Queen's University Belfast, Belfast BT7 1NN, UK.

b. Ångström Laboratory, Department of Chemistry, Uppsala University, Uppsala, Sweden

c. Institute of Physical Chemistry, Polish Academy of Sciences, Warsaw, Poland

d. Institute of Photonics and Quantum Sciences, Heriot-Watt University, Edinburgh EH14 4AS, UK.

e. Institute of Chemical Sciences, Heriot-Watt University, Edinburgh EH14 4AS, UK

† Corresponding author: j.greenwood@qub.ac.uk

Keywords: chirality; enantiomer excess; photoelectron spectroscopy; time-of-flight mass spectrometry; femtosecond laser ionization

Abstract

We present a proof-of-principle approach for discriminating chiral enantiomers based on the phenomenon of multiphoton photoelectron circular dichroism. A novel stereo detection setup was used to measure the number of photoelectrons emitted from chiral molecules in directions parallel or anti-parallel to the propagation of the ionising femtosecond laser pulses. In this study, we show how these asymmetries in the ketones camphor and fenchone depend upon the ellipticity of the laser pulses and the enantiomeric excess of the sample. By using a high repetition rate femtosecond laser, enantiomer excesses with uncertainties at the few-percent level could be measured in close to real-time. As the instrument is compact, and commercial turnkey femtosecond lasers are readily available, the development of a stand-alone chiral analysis instrument for a range of applications is now possible.

1. Introduction

Many molecules exhibit a specific handedness or chirality, a property which extends to biologically essential molecules such as amino acids and sugars. Molecular handedness directly influences organism response to the specific molecule since it determines how the molecule binds to a particular site on a receptor. Applications of advanced chemicals and pharmaceuticals necessitates the use of a pure active isomer, making the development of enantiomerically pure synthesis processes a persistent and extremely active research area. Detection of chiral excess post-reaction is an equally important but challenging proposition. Currently, there is not a simple, quick, and cost-effective method for chiral excess analysis that can be universally applied on a regular basis.

The difficulty is that the physical properties of enantiomeric pairs are almost identical or have very small differences, so that existing techniques such as optical rotation, circular dichroism (CD) and NMR peak height spectroscopy usually lack the speed, sensitivity and selectivity typically expected in analytical chemistry. Meanwhile, finding suitable host chiral compounds for identification by complexation or for the stationary phase in chiral chromatography usually has to be undertaken empirically on a case-by-case basis. As a result, there is considerable current research into alternative approaches which could be faster, more sensitive, and can be used on mixtures of compounds.

The discovery of a phenomenon known as photoelectron circular dichroism (PECD) has dramatically altered this landscape. Whereas conventional CD relies on very small differences in the excitation rates of electronic transitions between enantiomers (usually $< 0.1\%$), the asymmetry in photoelectron angular emission relative to the direction of light propagation from chiral enantiomers, has been found to be orders of magnitude higher (typically 10%). Since PECD is also measured with particle counting techniques in the gas phase, it potentially offers a route to chiral analysis with sensitivity and speed on a par or better than mass spectrometric chemical analysis. This PECD asymmetry has been investigated for single photon and multi-photon ionization through sophisticated velocity map imaging and analysis.

This asymmetry in the angular distribution of electrons is manifested via electric dipole transitions in the ionization process, hence it is orders of magnitude larger than conventional CD which depends on the

weak contribution from the magnetic dipole moment in the transition matrix [1,2,3]. The multiphoton PECD angular distributions are described by a partial wave expansion of the photoelectron wavefunction which results in an angular distribution with $2N$ terms (where N is the number of photons absorbed and P_i are Legendre polynomials).

$$I(\theta) = 1 + \sum_{i=1}^{2N} b_i \mathrm{P}_i(\cos\theta) \qquad (1)$$

It is the odd coefficients of this expansion b_i which produce the asymmetry in the forward-to-backward electron emission with respect to the light propagation direction. They are non-zero only for chiral molecules irradiated with circularly polarized light. Theoretical calculations and experimental verification of PECD were first conducted around 2000 for single photon ionization with vacuum ultraviolet radiation[4,5,6]. Subsequent studies have demonstrated PECD in a range of chiral molecules and for ionization of valence and core electrons[7,8,9,10,11,12,13]. The origin of the PECD asymmetry is attributed to the scattering of the outgoing electron wavefunction by the chiral potential of the molecule which, due to interferences, is sensitive to the emission energy, the initial orbital ionized, and small structural variations. However, the inherent asymmetry is primarily manifested through the simple ratio of photoemission into the forward and backward hemispheres, largely due to the b_1 coefficient. Therefore, we have developed a simple and elegant stereo-detection method by which the forward and backward emission rates are directly measured.

Most of these studies have been undertaken at synchrotron beamlines with adjustable helical undulators, which can produce left- or right-handed circularly polarized light[14,15]. Elliptically polarized light produced from high harmonics of optical lasers has also been successfully used for PECD measurements[16]. However, direct application of femtosecond lasers via multi-photon ionization PECD (MP-PECD) has also been established recently, which has opened up the possibility of a table-top analysis device.

By acquiring 2D projections with a velocity map imager and reconstructing the electron angular distribution, in 2012 Lux et al. were able to show a substantial asymmetry for the enantiomers of camphor

via resonant 2+1 photon ionization at 398 nm[17]. Similar results were acquired by Lehmann et al.[18] using a set-up for which the 3D distribution was obtained directly using a delay-line imaging detector. These groups have demonstrated PECD in a few other molecules, and by fitting the distributions with Legendre polynomials, the odd coefficients b_i arising from the chirality of the target were obtained[19,20,21,22,23,24,25]. The sensitivity of these parameters to molecular structure is evident for the isomers camphor and fenchone for which the b_1 coefficient has opposite signs.

From these formative studies it can be concluded that molecular chirality can be sensitively probed by the PECD b_i parameters through acquisition of the photoelectron's angular and energy distributions. However, such detailed information is not essential for identification of enantiomeric proportions or observing ultrafast chiral changes when a single parameter would be more expedient. Such a parameter (G) can be expressed through the ratio of the forward F (0°-90° to the laser propagation) to backward B (90°-180°) emission obtained from the integrated electron yields. In practice results are acquired for both left-(L) and right-hand(R) circularly polarized pulses to remove any instrumental asymmetries, so that G is defined as [18]

$$G = \frac{F_L - F_R}{(F_L + F_R)/2} - \frac{B_L - B_R}{(B_L + B_R)/2} \qquad (2)$$

This definition benefits from the fact that any instrumental asymmetry, such as differences in the detector efficiencies, is eliminated. As a result, it is not necessary to use sophisticated image detection and analysis to characterize the chirality of a sample when a simple stereo electron detection scheme could be just as effective. To this end we have developed a novel instrument which has been specifically designed to measure *G* values integrated over all electron energies of the forward and backward emitted electrons.

2. Experimental

A schematic of the experimental design is shown in Figure 1 [26]. Femtosecond laser pulses are focused through apertures into an interaction region which is sandwiched between two grounded rectangular plates where they intersect an effusive gas jet at room temperature. A magnetic field of 30-40 gauss is

applied along the laser propagation direction, so that photoelectrons spiral along the field lines with a net motion parallel or anti-parallel to the laser direction depending on whether they are emitted at less than or greater than 90°. Once the electrons have passed through grounded apertures at the entrance and exit of the interaction region, they are accelerated by a positive electric potential into **E** × **B** deflection plates which separate the electrons from the laser beam and direct them onto separate channel electron multipliers. In this way all the electrons emitted in each hemisphere are steered into their respective detectors regardless of their initial angle or energy.

The instrument can also be configured as a mass spectrometer with the two plates in the interaction region used to repel and extract the ions perpendicular to the laser direction into a short, linear time-of-flight tube. A microchannel plate was used to detect the ions and the mass spectra were used to confirm that photoelectrons were only being produced from the sample molecules. For the present results the instrument was set to detect either electrons or ions only, but simultaneous detection is possible if the interaction plates are pulsed after the electrons have left the interaction region. This coincidence detection mode will allow multiple component samples to be tested for chiral and chemical content concurrently. The potential of this type of analysis has been demonstrated previously for a velocity map imaging (VMI) set-up[27]. Although a VMI device provides highly detailed energy and angular information of the PECD, a position sensitive detector/imaging system and sophisticated analysis of the data is required. In the present innovative design, chiral analysis is also achieved, but by using a much simpler concept whereby the forward and backward emitted electrons are physically separated using magnetic and electric fields. As the electron detection is accomplished by two cheap, robust channel electron multipliers and the analysis required is very simple, the instrument is much smaller, costs less, and is capable of real-time analysis.

The number of counts obtained from left and right circularly polarized pulses in each detector were input into equation (2) to obtain values of the G parameter. Detailed information on the preparation of the laser pulses, samples and analysis can be found in the supporting information.

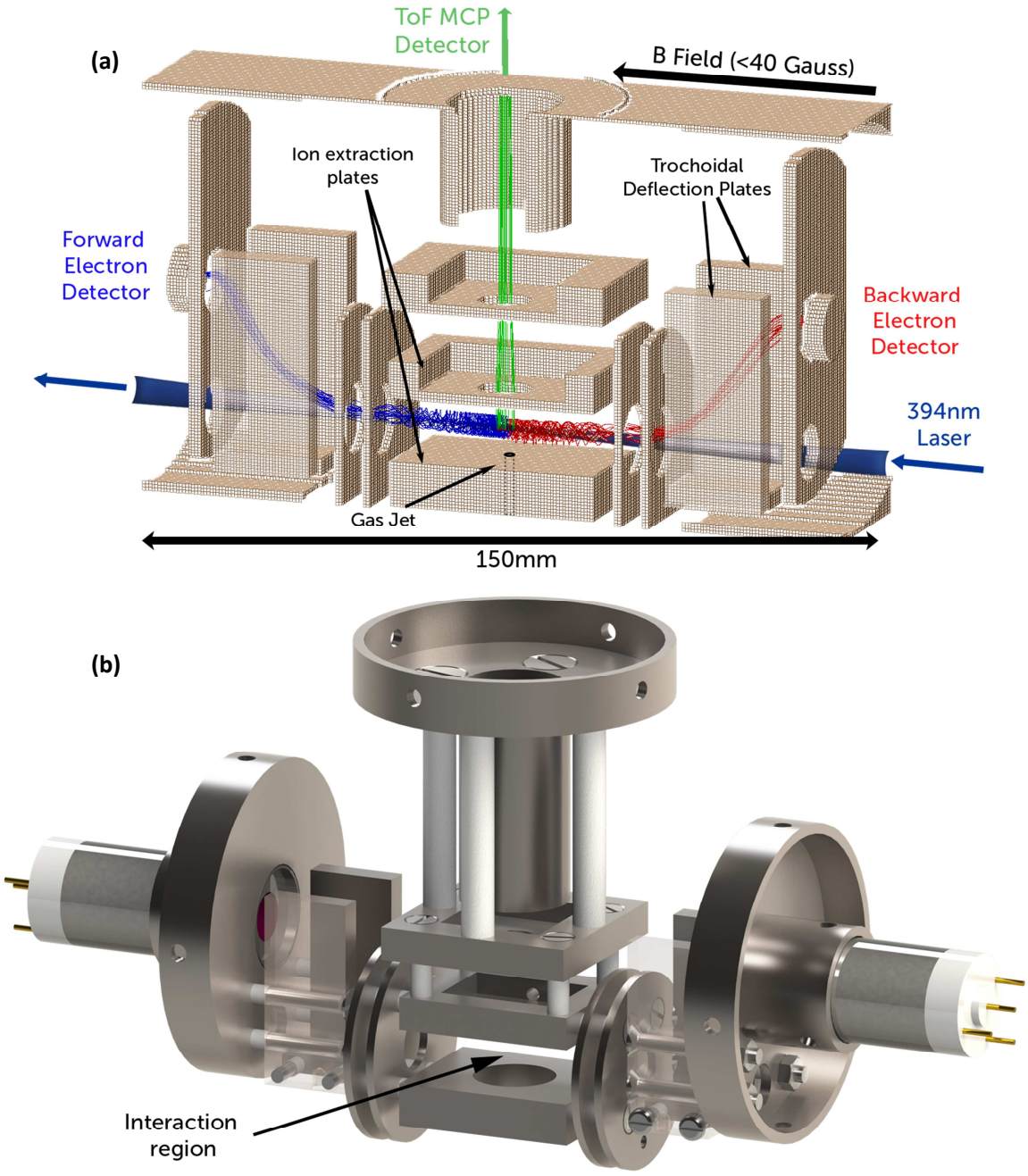

Figure 1: Schematics of the Interaction region of the instrument. (a) Simulated trajectories produced by SIMION 8.0 charge particle optics software[28]. Blue – forward emitted electrons, red – backward emitted electrons, green – ions. (b) 3D-CAD drawing of the mechanical design.

3. Results

The PECD asymmetries present in the enantiomers of the isomers camphor and fenchone were measured in this study. Both these molecules undergo 2+1 resonantly enhanced multiphoton ionisation at 394 nm. Results for the enantiomers of camphor and fenchone presented in Table 1 are in good agreement with the equivalent parameter measured in previous studies by the velocity map imaging technique. For the present measurements much lower intensities were used, mitigating saturation effects which can be a problem at higher intensities (see Table 1 and supplementary material of Lux et al.[19]).

Table 1: Current and previous G values for enantiomers of camphor and fenchone. Statistical uncertainties at the 2σ level are given for the present results. (*) Note that the current and previous results for R-fenchone used samples which were not enantiomerically pure.

Results	**G (%)**				**Wavelength (nm)**	**Pulse length (fs)**	**Intensity (Wcm^{-2})**
	Camphor		**Fenchone**				
	R	**S**	**R***	**S**			
Present	+8.1±0.5	-8.7±0.4	+9.2±0.6	-13.9±0.4	394	250	4×10^{10}
Lux et al.[17]	+6.9	-7.2			398	25	5×10^{13}
Lux et al.[19]	+8.0	-8.4	9.1	-10.1	398	25	4×10^{12}
Lehmann et al.[18]	+8.4	-7.4			400	150	$1\text{-}2 \times 10^{12}$
Kastner et al. [20]			-11.5	-14.25±0.1	398	25	2×10^{12}

It is noted that for fenchone there was no simple sign inversion of G for each enantiomer as values of +9.2 ± 0.6% for the R-enantiomer and -13.9 ± 0.4% for the S-enantiomer were obtained. When a 50:50 mix of these samples was measured, a G value of -2.0 ± 0.6% was obtained suggesting that the R sample was not enantiomerically pure. Assuming a pure S sample, we estimate that the R sample had an

enantiomeric excess of only 66 ± 5%. Lux et al.[19] and Nahon et al.[9] had a similar experience with their samples of R-fenchone.

PECD measurements of samples with different enantiomeric excesses have been undertaken in some previous measurements[9,19,20,27]. We have undertaken similar measurements in camphor but from samples with a greater range of proportions. The G values acquired from these samples are plotted in Figure 2. A straight line was fitted to this data with a gradient of 8.6 ± 0.3%. The intercept for this fit was zero within the uncertainties (–0.3 ± 0.3%), as would be expected for a racemic sample. This data demonstrates that any inherent instrumental asymmetry is completely eliminated and enantiomer excesses of 5% can be measured for acquisition times of less than a minute. Since this stereo-measurement does not require any complex processing, these results can also be updated in real time.

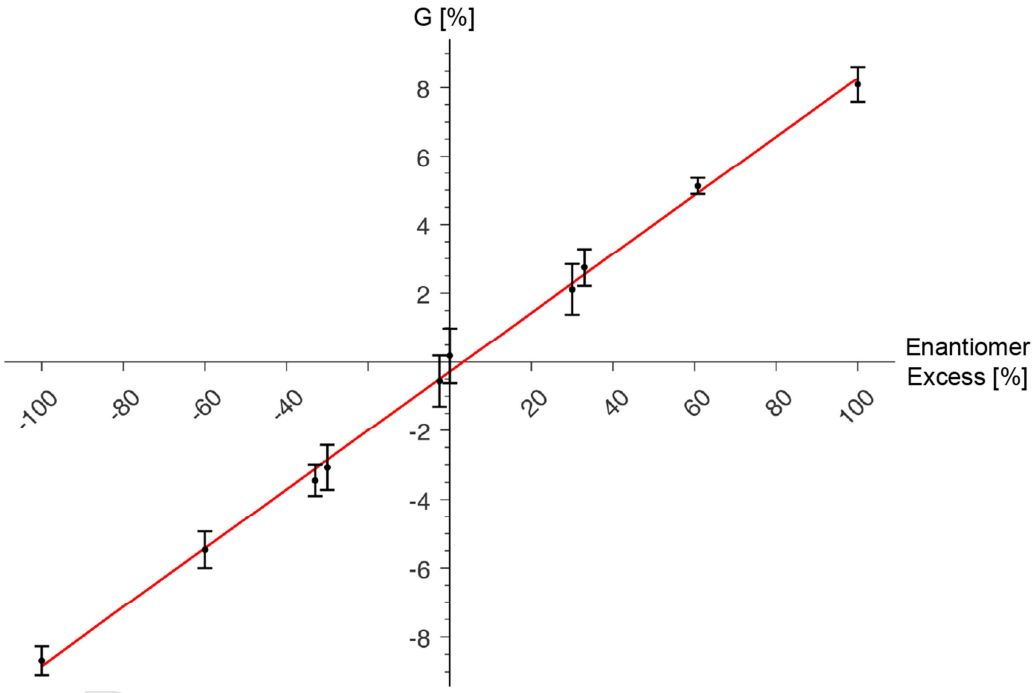

Figure 2: PECD G values for samples of camphor with different enantiomer excesses. For the highest signal rates, a 1σ statistical uncertainty of 0.2% could be obtained in an acquisition time of 15 minutes.

Further tests were performed to determine how G depends upon the degree of circular polarization of the pulses, by changing the angle of the quarter waveplate. These results are plotted in Figure 3 with respect to the Stokes S_3 parameter. As S_3 represents the difference in the intensity of the left to right circularly polarized components in the pulse, it might be expected that the graph has a linear dependence. However, while the trend for positive values of S_3 mirrors that for negative values as expected, G increases more rapidly for $|S_3| > 0.4$. Clearly detailed subtleties of the ionization process, such as selective excitation of certain molecular orientations in the ensemble must be influencing this non-linearity.

Previous ellipticity measurements by Lux et al.[19] for camphor showed a similar trend albeit they plotted a parameter which expresses the power rather than amplitude of the forward and backward angular distributions. Their data showed a sharp increase for $|S_3| > 0.99$ which might be equivalent to the apparent dip in the same region of our spectrum. The b_3 parameter was found to dominate the forward-backward asymmetry in camphor indicating that there is preferential excitation of molecules with a particular orientation. For perfectly circularly polarized pulses the propagation direction is the preferred axis of the coordinate system, but this symmetry is broken as the pulse gains a slight ellipticity and this could change the alignment of excited molecules. Therefore b_3 and hence G could be sensitive to $|S_3|$ when it is close to 1.

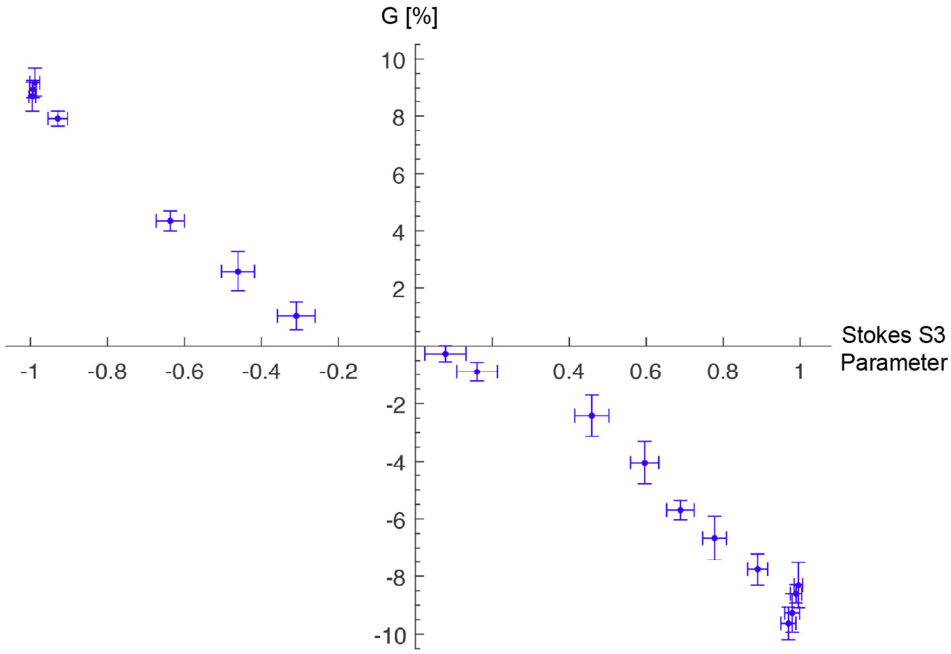

Figure 3: Variation in the G value for S-camphor as a function of the magnitude of the Stokes S_3 parameter.

4. Discussion

These results demonstrate that our instrument can measure enantiomer excesses more quickly and with a much higher sensitivity than conventional chiral analysis. It is also instructive to compare this performance with other laser based methods for chiral analysis which are currently being investigated. For instance measurements of the ion yields produced from femtosecond laser ionization have been used to distinguish enantiomers, but as the differences arise from the weak circular dichroism present in the excitation of an intermediate state, the asymmetry is generally smaller than PECD[29,30,31, 32,33,34,35,36]. Very intense laser pulses (10^{15} Wcm^{-2}) have also been used to directly identify the absolute enantiomer configuration from multi-coincidence detection of the coulomb explosion fragments produced following multiple ionization[37,38]. This has been demonstrated for some simple chiral molecules, but for larger systems the complexity of the dissociation processes would make accurate re-construction very

challenging. High harmonic spectra generated from femtosecond lasers with elliptical polarization have also been shown to be enantiomer dependent[39]. However, both these intense laser techniques rely on a chemically pure target and are unsuitable for multi-component samples.

An alternative scheme is based on microwave three-wave mixing for which the enantiomer sensitive phase of rotational transitions is measured[40,41]. This method is capable of determining enantiomer excesses of a few percent, and since the rotational excitation is resonant it can potentially be applied to chiral mixtures[42,43]. This is also a gas phase method but it will never be able to reach the sensitivities achievable through the single particle detection methods used in the present technique.

Since our device is compact, straightforward to operate, relatively low-cost, and can be easily coupled to any light source, it will open up more extensive investigations and applications of PECD. As well as contributing to fundamental studies of PECD, particularly as new theoretical codes begin to tackle this complex phenomenon[44,45,46,47], this technique could also exploit the sensitivity of the G parameter to track ultrafast electronic or structural changes in molecules[48,49]. For example, as high harmonic and free electron laser sources of circularly polarized light become available[50,51], processes such as photoisomerization and charge migration, could be observed on femtosecond or even attosecond timescales. In addition, the recent observation of PECD in the tunnelling regime[52] shows that an intermediate resonance is not essential, thus making this chiral analysis instrument highly versatile.

In this communication we have also demonstrated that fast, sensitive measurements of enantiomer excess are possible for practical applications. Indeed if a laser with higher pulse energy and repetition rate was used, the acquisition times could be further reduced enabling real time analysis. Although the present study has focused on pure samples, the instrument has the capability of running in an electron-ion coincidence mode so that acquisition of enantiomer analyzed mass spectra will be possible in the future. Given that detection of organic molecules at parts per trillion concentrations and limits of detection of a few attomoles are achievable with femtosecond laser ion sources[53], this could open up a new paradigm in chiral analysis. One could envisage such an instrument being used to test trace amounts of material in environmental, food, or medical samples without substantial pre-processing, or to analyze and optimize

the synthesis of chiral compounds. With the dramatic advances in commercial, high power, high repetition rate femtosecond fiber laser technology, such applications could become a reality in the next few years.

Acknowledgements

This work was supported by the the Leverhulme Trust (RPG-2012-735) and the UK's Engineering and Physical Sciences Research Council (EP/M001644/1). JM acknowledges support from the EU COST Action CM1405 – *Molecules in Motion* (MOLIM) and the Northern Ireland Department of Employment and Learning.

[1] B. Ritchie, Theory of the angular distribution of photoelectrons ejected from optically active molecules and molecular negative ions. *Phys. Rev. A*, **13**, 1411 (1976)
[2] I. Powis, Photoelectron circular dichroism in chiral molecules. *Adv. Chem. Phys*., **138**, 267 (2008)
[3] L. Nahon, G. A. Garcia and I. Powis, Two-dimensional charged particle image inversion using a polar basis function expansion. *J. Elect. Spect. Rel. Phenom*., **204**, 322 (2015)
[4] I. Powis, Photoelectron circular dichroism of the randomly oriented chiral molecules glyceraldehyde and lactic acid. *J. Chem. Phys.*, **112**, 301 (2000)
[5] I. Powis, Photoelectron spectroscopy and circular dichroism in chiral biomolecules: L-alanine. *J. Phys. Chem. A*, **104**, 878 (2000)
[6] N. Böwering, T. Lischke, B. Schmidtke, N. Müller, T. Khalil and U. Heinzmann, Asymmetry in photoelectron emission from chiral molecules induced by circularly polarized light . *Phys. Rev. Lett*., **86**, 1187 (2001)
[7] S. Turchini, N. Zema, G. Contini, G. Alberti, M. Alagia, S. Stranges, G. Fronzoni, M. Stener, P. Decleva, and T. Prosperi, Circular dichroism in photoelectron spectroscopy of free chiral molecules: Experiment and theory on methyl-oxirane. *Phys. Rev. A*, **70**, 014502 (2004)
[8] C. J. Harding, E. Mikajlo, I. Powis, S. Barth, S. Joshi, V. Ulrich and U. Hergenhahn, Circular dichroism in the angle-resolved C 1s photoemission spectra of gas-phase carvone enantiomers. *J. Chem. Phys*., **123**, 234310 (2005)
[9] L. Nahon, L. Nag, G. A. Garcia, I. Myrgorodska, U. Meierhenrich, S. Beaulieu, V. Wanie, V. Blanchet, R. Géneaux and I. Powis, Determination of accurate electron chiral asymmetries in fenchone and camphor in the VUV range: sensitivity to isomerism and enantiomeric purity. *Phys.Chem.Chem.Phys.*, **18**, 12696 (2016)
[10] G Prümper, T Lischke, H Fukuzawa, A Reinköster and K Ueda, Upper limits for the circular dichroism for the C 1s and O 1s core excitation of methyl oxirane. *J. Phys. B*, **40**, 3425 (2007)
[11] V. Ulrich, S. Barth, S. Joshi and U. Hergenhahn, Giant Chiral Asymmetry in the C 1 s Core Level Photoemission from Randomly Oriented Fenchone Enantiomers. *J. Phys. Chem. A*, **112**, 3544 (2008)
[12] G. A. Garcia, L. Nahon, S. Daly and I. Powis, Vibrationally induced inversion of photoelectron forward-backward asymmetry in chiral molecule photoionization by circularly polarized light. *Nat. Comm.*, **4**, 2132 (2013)
[13] M. Tia, B. Cunha de Miranda, S. Daly, F. Gaie-Levrel, G. A. Garcia, L. Nahon and I. Powis, VUV photodynamics and chiral asymmetry in the photoionization of gas phase alanine enantiomers. *J. Phys. Chem. A*, **118**, 2765 (2014)
[14] L. Nahon, N. de Oliveira, G. A. Garcia, J.-F. Gil, B. Pilette, O. Marcouillé, B. Lagarde and F. Polack, DESIRS: a state-of-the-art VUV beamline featuring high resolution and variable polarization for spectroscopy and dichroism at SOLEIL. *J. Synchrotron Rad*., 19, 508 (2012)
[15] A. A. Lutman et al., Polarization control in an X-ray free-electron laser. *Nat. Phot.*, **10**, 468 (2016)
[16] A. Ferre, C. Handschin, M. Dumergue, F. Burgy, A. Comby, D. Descamps, B. Fabre, G. A. Garcia, R. Géneaux, L. Merceron, E. Mével, L. Nahon, S. Petit, B. Pons, D. Staedter, S. Weber, T. Ruchon, V. Blanchet and Y. Mairesse, A table-top ultrashort light source in the extreme ultraviolet for circular dichroism experiments. *Nat. Phot.*, **9**, 93 (2015)

[17] C. Lux, M. Wollenhaupt, T. Bolze, Q. Liang, J. Kohler, C. Sarpe and T. Baumert, Circular dichroism in the photoelectron angular distributions of camphor and fenchone from multiphoton ionization with femtosecond laser pulses. *Angew. Chem. Int. Ed*., **51**, 1 (2012)
[18] C.S. Lehmann, N. B. Ram, I. Powis, and M. H. M. Janssen, Imaging photoelectron circular dichroism of chiral molecules by femtosecond multiphoton coincidence detection. *J. Chem. Phys.*, **139**, 234307 (2013)
[19] C. Lux, M. Wollenhaupt, C. Sarpe and T. Baumert, Photoelectron circular dichroism of bicyclic ketones from multiphoton ionization with femtosecond laser pulses. *ChemPhysChem*, **16**, 115 (2015)
[20] A. Kastner, C. Lux, T. Ring, S. Züllighoven, C. Sarpe, A. Senftleben and T. Baumert, Enantiomeric Excess Sensitivity to Below One Percent by Using Femtosecond Photoelectron Circular Dichroism. *ChemPhysChem*, **17**, 1119 (2016)
[21] C. Lux, A. Senftleben, C. Sarpe, M. Wollenhaupt and T. Baumert, *J. Phys. B*, **49**, 02LT01 (2016)
[22] M. H. M. Janssen and I. Powis, Detecting chirality in molecules by imaging photoelectron circular dichroism. *Phys. Chem. Chem. Phys*., **16**, 856 (2014)
[23] M. F. R. Fanood, I. Powis and M. H. M. Janssen, Chiral Asymmetry in the Multiphoton Ionization of Methyloxirane Using Femtosecond Electron–Ion Coincidence Imaging . *J. Phys. Chem. A*, **118**, 11541 (2014)
[24] M. F. R. Fanood, M. H. M. Janssen and I. Powis, Enantioselective femtosecond laser photoionization spectrometry of limonene using photoelectron circular dichroism. *Phys. Chem. Chem. Phys.*, **17**, 8614 (2015)
[25] M. F. R. Fanood, I. Powis and M. H. M. Janssen, Wavelength dependent photoelectron circular dichroism of limonene studied by femtosecond multiphoton laser ionization and electron-ion coincidence imaging, *J. Chem. Phys*., **145**, 124320 (2016)
[26] Patent applied for
[27] M. F. R. Fanood, N. B. Ram, C. S. Lehmann, I. Powis and M. H. M. Janssen, Enantiomer-specific analysis of multi-component mixtures by correlated electron imaging-ion mass spectrometry. *Nat. Comm.*, **6**, 7511 (2015)
[28] SIMION 8.0.4, D. Manura, Scientific Instrument Services Inc.(2008)
[29] U. Boesl and A. Bornschlegl, Circular Dichroism Laser Mass Spectrometry: Differentiation of 3□Methylcyclopentanone Enantiomers. *ChemPhysChem*, **7**, 2085 (2006)
[30] C. Logé and U. Boesl, Laser mass spectrometry with circularly polarized light: two-photon circular dichroism. *Phys. Chem. Chem. Phys.*, **14**, 11981 (2012)
[31] U. Boesl, A. Bornschlegl, C. Logé and K. Titze, Resonance-enhanced multiphoton ionization with circularly polarized light: chiral carbonyls. *Anal Bioanal Chem.*, **405**, 6913 (2013)
[32] K. Titze, T. Zollitsch, U. Heiz and U. Boesl, Laser mass spectrometry with circularly polarized light: circular dichroism of cold molecules in a supersonic gas beam. *ChemPhysChem*, **15**, 2762 (2014)
[33] P. Horsch, G. Urbasch, K.-M. Weitzel and D. Kröner, Circular dichroism in ion yields employing femtosecond laser ionization—the role of laser pulse duration. *Phys. Chem. Chem. Phys.*, **13**, 2378 (2011)
[34] P. Horsch, G. Urbasch and K.-M. Weitzel, Analysis of chirality by femtosecond laser ionization mass spectrometry. *Chirality*, **24**, 684 (2012)
[35] A. Hong, C. M. Choi, H. J. Eun, C. Jeong, J. Heo and N. J. Kim, Conformation□specific circular dichroism spectroscopy of cold, isolated chiral molecules. *Angew. Chem. Int. Ed*., **53**, 7805 (2014)
[36] U. Bosel and A. Kartouzian, Mass-Selective Chiral Analysis, *Annual Rev. Anal. Chem*., **9**, 343 (2016)
[37] M. Pitzer, M. Kunitski, A. S. Johnson, T. Jahnke, H. Sann, F. Sturm, L. Ph. H. Schmidt, H. Schmidt-Böcking, R. Dörner, J. Stohner, J. Kiedrowski, M. Reggelin, S. Marquardt, A. Schießer, R. Berger, M. S. Schöffler, Absolute configuration from different multifragmentation pathways in light□induced coulomb explosion imaging. *Science*, **341**, 1096 (2013)
[38] L. Christensen, J. H. Nielsen, C. S. Slater, A. Lauer and M. Brouard, H. Stapelfeldt, Using laser-induced Coulomb explosion of aligned chiral molecules to determine their absolute configuration. *Phys. Rev. A*, **92**, 033411 (2015)
[39] R. Cireasa, A. E. Boguslavskiy, B. Pons, M. C. H. Wong, D. Descamps, S. Petit, H. Ruf, N. Thiré1, A. Ferré, J. Suarez, J. Higuet, B. E. Schmidt, A. F. Alharbi, F. Légaré, V. Blanchet, B. Fabre, S. Patchkovskii, O. Smirnova, Y. Mairesse and V. R. Bhardwaj, Probing molecular chirality on a sub-femtosecond timescale, *Nat. Phys*. 11, 654-658 (2015)
[40] D. Patterson, M. Schnell and J. M. Doyle, Enantiomer-specific detection of chiral molecules via microwave spectroscopy. *Nature*, **497**, 475 (2013)
[41] V. A. Shubert, D. Schmitz, C. Pérez, C. Medcraft, A. Krin, S. R. Domingos, D. Patterson and M. Schnell, Chiral analysis using broadband rotational spectroscopy. *J. Phys. Chem. Lett.*, **7**, 341 (2016)
[42] D. Patterson and M. Schnell, New studies on molecular chirality in the gas phase: enantiomer differentiation and determination of enantiomeric excess. *Phys.Chem.Chem.Phys.*, **16**, 11114 (2014)
[43] V. A. Shubert, D. Schmitz, D. Patterson, J. M. Doyle and M. Schnell, Identifying enantiomers in mixtures of chiral molecules with broadband microwave spectroscopy. *Angew. Chem. Int. Ed*., **53**, 1152 (2014)
[44] I. Dreissigacker and M. Lein, Photoelectron circular dichroism of chiral molecules studied with a continuum-state-corrected strong-field approximation. *Phys. Rev. A*, **89**, 053406 (2014)
[45] A. N. Artemyev, A. D. Müller, D. Hochstuhl, and P. V. Demekhin, Photoelectron circular dichroism in the multiphoton ionization by short laser pulses. I. Propagation of single-active-electron wave packets in chiral pseudo-potentials. *J. Chem. Phys.*, **142**, 244105 (2015)
[46] A. Wardlow and D. Dundas, High-order-harmonic generation in benzene with linearly and circularly polarized laser pulses. *Phys. Rev. A*, **93**, 023428 (2016)

[47] R. E. Goetz, T. A. Isaev, B. Nikoobakht, R. Berger, and C. P. Koch, Theoretical description of circular dichroism in photoelectron angular distributions of randomly oriented chiral molecules after multi-photon photoionization. arXiv:1606.04436v1 [quant-ph] (2016)
[48] S. Beaulieu, A. Comby, B. Fabre, D. Descamps, A. Ferré, G. Garcia, R. Géneaux, F. Légaré, L. Nahon, S. Petit, T. Ruchon, B. Pons, V. Blanchet and Y. Mairesse, Probing ultrafast dynamics of chiral molecules using time-resolved photoelectron circular dichroism, *Faraday Discuss*., **194**, 325-348 (2016)
[49] A. Comby, S. Beaulieu, M. Boggio-Pasqua, D. Descamps, F. Légaré, L. Nahon, S. Petit, B. Pons, B. Fabre, Y. Mairesse and V. Blanchet, Relaxation Dynamics in Photoexcited Chiral Molecules Studied by Time-Resolved Photoelectron Circular Dichroism: Toward Chiral Femtochemistry, *J. Phys. Chem. Lett*., **7**, 4514 (2016)
[50] O. Kfir, P. Grychtol, E. Turgut, R. Knut, D. Zusin, D. Popmintchev, T. Popmintchev, H. Nembach, J. M. Shaw, A. Fleischer, H. Kapteyn, M. Murnane and O. Cohen, Generation of bright phase-matched circularly-polarized extreme ultraviolet high harmonics. *Nat. Phot.*, **9**, 93 (2015)
[51] C. Spezzani, E. Allaria, M. Coreno, B. Diviacco, E. Ferrari, G. Geloni, E. Karantzoulis, B. Mahieu, M. Vento, and G. De Ninno, Coherent light with tunable polarization from single-pass free-electron lasers. *Phys. Rev. Lett.*, **107**, 084801 (2011)
[52] S. Beaulieu, A. Ferré, R. Géneaux, R. Canonge, D. Descamps, B. Fabre, N. Fedorov, F. Légaré, S. Petit, T. Ruchon, V. Blanchet, Y. Mairesse and B. Pons, Universality of photoelectron circular dichroism in the photoionization of chiral molecules *New J. Phys*., **18**, 102002 (2016)
[53] J. Miles, S. De Camillis, G. Alexander, K. Hamilton, T. J. Kelly, J. T. Costello, M. Zepf, I. D. Williams, and J. B. Greenwood, Detection limits of organic compounds achievable with intense, short-pulse lasers. *Analyst*, **140**, 4270 (2015)